

# Megacity Emissions and Lifetimes of Nitrogen Oxides Probed from Space

Steffen Beirle,<sup>1\*</sup> K. Folkert Boersma,<sup>2,3</sup> Ulrich Platt,<sup>4</sup> Mark G. Lawrence,<sup>1</sup> Thomas Wagner<sup>1</sup>

Megacities are immense sources of air pollutants, with large impacts on air quality and climate. However, emission inventories in many of them still are highly uncertain, particularly in developing countries. Satellite observations allow top-down estimates of emissions to be made for nitrogen oxides ( $\text{NO}_x = \text{NO} + \text{NO}_2$ ), but require poorly quantified a priori information on the  $\text{NO}_x$  lifetime. We present a method for the simultaneous determination of megacity  $\text{NO}_x$  emissions and lifetimes from satellite measurements by analyzing the downwind patterns of  $\text{NO}_2$  separately for different wind conditions. Daytime lifetimes are  $\sim 4$  hours at low and mid-latitudes, but  $\sim 8$  hours in wintertime for Moscow. The derived  $\text{NO}_x$  emissions are generally in good agreement with existing emission inventories, but are higher by a factor of 3 for the Saudi Arabian capital Riyadh.

**N**itrogen oxides, which are produced mostly by combustion processes, play a key role in tropospheric chemistry: They are toxic, contribute to acid rain, can act as aerosol precursors, and are catalysts for ozone formation (“summer smog”) (1). Thus, global and regional chemistry models require accurate  $\text{NO}_x$  emission inventories, in particular for megacities (2), which are immense sources of numerous pollutants (3–5). However, substantial differences among state-of-the-art emission databases have been found (6), and uncertainties are high (7).

Satellite measurements of  $\text{NO}_2$  tropospheric columns have revolutionized our insight into the distribution and magnitude of sources of nitrogen oxides over the past decade (8–14) and generally enable top-down  $\text{NO}_x$  emission estimates on regional and global scales (8–10). This, however, requires a priori information on the  $\text{NO}_x$  lifetime  $\tau$ , which, at daytime, is mainly determined by the reaction of  $\text{NO}_2$  with the hydroxyl radical OH, leading to formation of  $\text{HNO}_3$  (15).  $\tau$  can generally be obtained from atmospheric chemistry models (16), but the accuracy of the estimated emissions is then limited by the models’ capability to represent OH concentrations accurately, which is especially difficult for megacities owing to highly nonlinear small-scale chemistry.

For typical background OH concentrations ( $\sim 10^6$  molecules/ $\text{cm}^3$ ),  $\tau$  is about a day (1), but within pollution plumes with active photochemistry and enhanced OH levels, it is only a

few hours, as determined by measuring the downwind evolution of  $\text{NO}_x$  during aircraft transects of plumes from cities and power plants (17, 18). Similar lifetime information can also be gained from the downwind evolution of  $\text{NO}_2$  as observed from satellite instruments (8, 13, 19) (20).

Here we present a method for the simultaneous determination of  $\text{NO}_x$  emissions and lifetimes for megacities and other strong “point” sources. In contrast to earlier analyses of satellite data, this investigation of photochemistry within urban plumes was rendered possible by the spatial resolution of the Ozone Monitoring Instrument (OMI) (21) with ground pixel sizes down to 24 km by 13 km.

The essential element of our approach is that the mean  $\text{NO}_2$  distribution is calculated separately for different wind direction sectors, rather than taking the overall average. By making this separation, we avoid the neutralization of outflow patterns of opposite wind directions, which would result in low average wind speeds and rather symmetric  $\text{NO}_2$  patterns. Instead, situations with high mean winds (for each wind direction sector considered separately) and correspondingly distinct outflow patterns are achieved.

In this study, we consider OMI  $\text{NO}_2$  tropospheric columns, i.e., vertically integrated concentrations, from “cloud free” (cloud fraction below 30%) measurements at  $\sim 2$  p.m. local time for 2005 to 2009 (v1.02, TEMIS) (22). Each OMI ground pixel is linked to wind data (below 500 m) from the European Centre for Medium-Range Weather Forecasts (ECMWF) (23). For details see (24).

To demonstrate our approach, we focus on Riyadh, the capital of Saudi Arabia, with a population of about 5 million (city) to 7 million

<sup>1</sup>Max-Planck-Institut für Chemie, Joh.-Joachim-Becherweg 27, 55128 Mainz, Germany. <sup>2</sup>Koninklijk Nederlands Meteorologisch Instituut, Wilhelminalaan 10, 3732 GK De Bilt, Netherlands. <sup>3</sup>Eindhoven University of Technology, Den Dolech 2, 5612 AZ Eindhoven, Netherlands. <sup>4</sup>Institut für Umweltphysik, Universität Heidelberg, INF 229, 69120 Heidelberg, Germany.

\*To whom correspondence should be addressed. E-mail: steffen.beirle@mpic.de

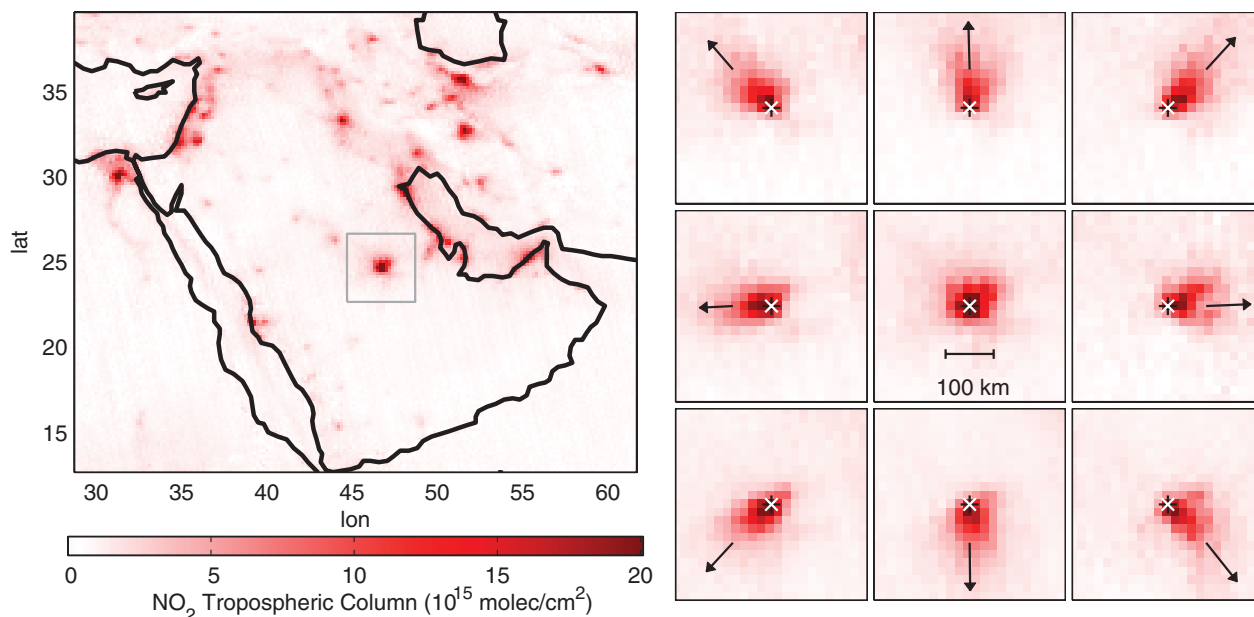


**Fig. 1.** Wind dependency of  $\text{NO}_2$  column densities around Riyadh. **(Left)** Mean  $\text{NO}_2$  tropospheric columns in the Middle East from OMI measurements during 2005 to 2009 for calm ( $w < 2$  m/s) conditions with  $< 30\%$  cloud cover. The gray box indicates the area around Riyadh displayed in the enlarged

plots on the right. **(Right)** Mean  $\text{NO}_2$  column densities around Riyadh (white cross) for different wind conditions, i.e., calm (center panel) and eight main wind direction sectors (surrounding panels; arrows indicate the mean of the respective ECMWF winds).

(greater area) inhabitants. Riyadh is particularly suited for this study for several reasons: First,  $\text{NO}_2$  tropospheric columns in Riyadh are large ( $\sim 20 \times 10^{15}$  molecules/ $\text{cm}^2$ ). Second, Riyadh is isolated (no other large  $\text{NO}_x$  sources within  $\sim 200$  km radius), and the contrast between the polluted city center and the relatively low background ( $\sim 1 \times 10^{15}$  molecules/ $\text{cm}^2$ ) is high. Thus, Riyadh can be considered as a nearly idealized point source of  $\text{NO}_x$ . Third, Riyadh is far from the coast, and the surrounding terrain, and thus also wind fields, are rather homogeneous. Finally, Riyadh is only rarely covered by clouds, allowing undisturbed satellite observations down to the ground.

Figure 1 (left) displays mean  $\text{NO}_2$  tropospheric columns for the Middle East region for calm conditions (wind speeds  $w < 2$  m/s). On the right, enlarged plots for Riyadh and the surrounding area are shown, where  $\text{NO}_2$  tropospheric columns have been averaged separately for different wind direction sectors (southeast, south, southwest, etc.); each OMI measurement is assigned to one of these sectors according to the respective ECMWF average wind direction below 500 m. The resulting spatial patterns clearly illustrate the outflow of  $\text{NO}_2$  from Riyadh, consistent with ECMWF winds. In the analysis below, each OMI observation (also for  $w < 2$  m/s) is assigned to a wind direction sector, to increase sample sizes and reduce noise.

For each wind direction sector, the mean column density maps (two-dimensional, 2D) are reduced to 1D “line densities” along the respective main wind direction ( $x$ ) by integration across the wind direction ( $y$ ), respectively (fig. S1). The integration implicitly accounts at the same time for the spatial extent of the source, the OMI ground pixel size, and wind velocity fluctuations in the  $y$  direction. Figure 2 shows line densities (light colors) as a function of the distance  $x$  to the Riyadh city center, exemplarily for easterly (red) and westerly (blue) winds. A clear asymmetry of the spatial patterns due to transport can be seen: The maximum is shifted in the wind direction, and the curve is less steep downwind than upwind.

Assuming a pseudo first-order loss of  $\text{NO}_2$ , the mean  $\text{NO}_x$  lifetime  $\tau_{\text{NO}_x}$  and  $\text{NO}_x$  emissions  $E_{\text{NO}_x}$  can be determined from the observed downwind decay. For this purpose, we perform a non-linear least-squares fit of a simple model function  $M(x)$  (dark colors in Fig. 2) to the observed spatial pattern of the  $\text{NO}_2$  line density, as a function of the distance  $x$ .  $M(x)$  describes, in essence, a spatially smoothed exponential downwind decay (24). Fitted parameters are the  $e$ -folding distance  $x_0$ , the spatial smoothing parameter  $\sigma$ , the location of the apparent point source relative to the city center  $X$ , total emissions  $E$ , and a constant background  $B$ .  $\sigma$  accounts for any kind of spatial smoothing in the main wind direction, caused by the actual spatial extent of the source, the ground pixel size of OMI observations with different spatial samplings, and wind variations. For details, see (24).

For Riyadh, the observed mean downwind patterns can be described successfully by this simple model function: Correlation coefficients between observation and fit are about  $R^2 = 0.98$  for all wind direction sectors. From the fitted  $e$ -folding distance  $x_0$ , the mean daytime lifetime  $\tau$  is derived by division by the mean wind speed  $w$ . This actually reflects the  $\text{NO}_x$  lifetime, as long as the  $[\text{NO}_2]/[\text{NO}_x]$  ratio does not change much within the downwind plume (17). For each wind direction sector,  $\tau$  is computed to be about 4 hours with a typical 95% confidence interval (CI) of about  $\pm 0.5$  hours. Averaging the fit results for all wind direction sectors yields  $\tau = 4.0$  hours with a standard mean error (SME) of 0.4 hours.

The derived emissions  $E$  (in terms of  $\text{NO}_2$ ) are  $187 \pm 14$  mol/s (mean  $\pm$  SME) with a typical CI of 16 mol/s for the individual wind direction

sectors. For the determination of  $\text{NO}_x$  emissions  $E_{\text{NO}_x}$ ,  $E$  is scaled by a factor of 1.32, according to typical  $[\text{NO}]/[\text{NO}_2]$  ratios of 0.32 under urban conditions at noon (1). The other fitted parameters are  $X = 15 \pm 4$  km,  $B = (0.27 \pm 0.03) \times 10^{23}$  molecules/cm, which corresponds to a background tropospheric column of  $(1.1 \pm 0.1) \times 10^{15}$  molecules/ $\text{cm}^2$ , and  $\sigma = 21 \pm 1$  km, which is of the expected order of magnitude according to the spatial extent of Riyadh and the OMI ground pixel size.

The CI and SME reflect the fit performance and the consistency of the result for the different wind direction sectors, respectively, and both can be regarded as measures of uncertainty. In addition, the absolute values for  $E$  (but not  $\tau$ ) are also directly affected by the uncertainty of OMI tropospheric columns of about 30% (22), as well as by the uncertainty in the  $\text{NO}_x/\text{NO}_2$  scaling

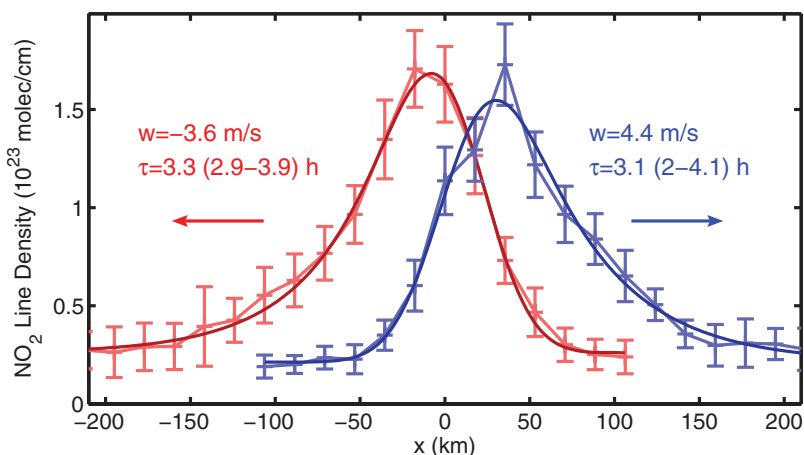
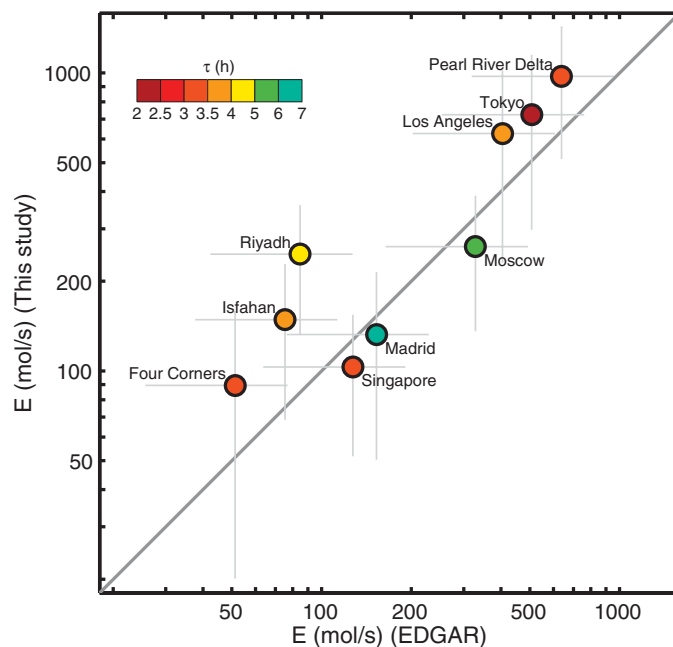


**Fig. 2.** Downwind evolution of  $\text{NO}_2$ . Light colors: Zonally integrated  $\text{NO}_2$  column densities (mean  $\pm$  SME) for westerly (blue) and easterly (red) winds as function of the distance to Riyadh City center  $x$ . Dark colors: the respective fit result  $M(x)$ . The numbers indicate the mean wind velocities from ECMWF ( $w$ ) and the lifetimes  $\tau$  resulting from the least-squares fit with 95% CIs.

**Fig. 3.** Resulting  $\text{NO}_x$  emissions and lifetimes. Scatterplot of the resulting  $\text{NO}_x$  emissions for the considered megacities and power plants versus the respective EDGAR emissions (V4.1, integrated over 250 km by 250 km). Error bars show the total uncertainties for  $E_{\text{NO}_x}$  (24), whereas EDGAR errors are set to 50% according to the expert judgment (“medium magnitude of uncertainty”) (7). Resulting  $\text{NO}_x$  lifetimes are color coded.



factor (~10%). Further sources of uncertainty of both  $\tau$  and  $E$  are the settings applied for spatial integration (~10%) (fig. S2) and the choice of wind data (~30%). Total errors of  $\tau$  and  $E$  are estimated as the quadratic sum of these uncertainties, assuming them to be independent (24).

Our method for determining  $\text{NO}_x$  lifetimes and emissions is generally applicable for a strong, localized source. Figure 3 compares the resulting  $\text{NO}_x$  emissions to the EDGAR (V4.1) emission inventory (25, 26) for the year 2005 for a set of (mega)cities and one other strong point source, the Four Corners (27) power plants, which have passed an automated performance check (see SOM text and table S1). In addition, the derived mean lifetimes are color-coded in the scatterplot.

Despite the large uncertainties on the order of 50% for both our results and EDGAR emissions (7), the derived emissions are generally in good agreement with the EDGAR inventory. One possible reason for the deviations is that, due to the short lifetimes, our method is only sensitive to daytime emissions (see SOM text and fig. S4), whereas EDGAR emissions are 24-hour annual averages. For Riyadh, however, where our fit performs best, resulting emissions are higher by a factor of 3. This indicates that EDGAR  $\text{NO}_x$  emissions are too low for Riyadh, though the reason for this is not yet clear; however, from a trend analysis of the satellite observations, we can exclude that this discrepancy is just due to emission changes since the EDGAR reference year of 2005.

The simultaneously derived daytime lifetimes are almost free of a priori assumptions or model input, as they are based on the relative downwind patterns. They are in the range of 2.3 to 6.4 hours (with typical uncertainties of 40 to 60%), in good agreement with prior measurements (16, 17). This range constrains the average OH concentration to be between about  $10 \times 10^6$  and  $4 \times 10^6$  molecules/cm<sup>3</sup>. This directly reflects the oxidizing capacity within the fresh urban plume, which is

also relevant for the depletion of other pollutants like CO, SO<sub>2</sub>, and volatile organic compounds.

An additional analysis of seasonal mean lifetimes and emissions generally reveals similar results (fig. S3). But at higher latitudes (Moscow) in winter, when heterogeneous night-time reactions of  $\text{NO}_x$  (i.e., conversion to  $\text{HNO}_3$  via  $\text{NO}_3$  and  $\text{N}_2\text{O}_5$ ) are probably the dominating loss processes, the derived lifetimes are considerably longer (8 hours).

Owing to the global coverage of satellite observations, our method can be applied to various major “point sources” such as megacities around the world. With the ongoing time series of current and especially future (geostationary) satellite instruments with better spatial resolution, our method can serve as a robust, independent tool to validate  $\text{NO}_x$  emission inventories of megacities, and might also be applied to other trace gases in the future as retrievals continue to improve.

#### References and Notes

- J. H. Seinfeld, S. N. Pandis, *Atmospheric Chemistry and Physics* (Wiley, New York, ed. 2, 2006).
- In this study, we define “megacity” as a city with more than 5 million inhabitants, following the definition used within the MEGAPOLI project ([http://megapoli.dmi.dk/nlet/MEGAPOLI\\_NewsLet01.pdf](http://megapoli.dmi.dk/nlet/MEGAPOLI_NewsLet01.pdf)).
- M. Molina, L. Molina, *J. Air Waste Manage. Assoc.* **54**, 644 (2004).
- M. G. Lawrence, T. M. Butler, J. Steinkamp, B. R. Gurjar, J. Lelieveld, *Atmos. Chem. Phys.* **7**, 3969 (2007).
- D. Butler, *Nature* **455**, 142 (2008).
- T. M. Butler *et al.*, *Atmos. Environ.* **42**, 703 (2008).
- EDGAR, available at <http://themasites.pbl.nl/en/themasites/edgar/documentation/uncertainties/index.html>.
- C. Leue *et al.*, *J. Geophys. Res.* **106**, (D6), 5493 (2001).
- R. V. Martin *et al.*, *J. Geophys. Res.* **108**, 4537 (2003).
- I. B. Kononov, M. Beekmann, A. Richter, J. P. Burrows, *Atmos. Chem. Phys.* **6**, 1747 (2006).
- A. Richter, J. P. Burrows, H. Nüss, C. Granier, U. Niemeier, *Nature* **437**, 129 (2005).
- S. Beirle, U. Platt, M. Wenig, T. Wagner, *Atmos. Chem. Phys.* **3**, 2225 (2003).
- S. Beirle, U. Platt, R. von Glasow, M. Wenig, T. Wagner, *Geophys. Res. Lett.* **31**, L18102 (2004).

- R. Martin, *Atmos. Environ.* **42**, 7823 (2008).
- Other loss processes are, e.g., wet and dry deposition and the formation of peroxyacetyl nitrate (PAN).
- Either explicitly, or implicitly via inverse modeling approaches.
- C. W. Spicer, *Science* **215**, 1095 (1982).
- T. B. Ryerson *et al.*, *J. Geophys. Res.* **103**, 22569 (1998).
- T. Kunhikrishnan *et al.*, *Atmos. Environ.* **38**, 581 (2004).
- Because the respective satellites have repeat cycles of only 1 to 6 days, it is generally not possible to track a particular air mass, as done with in situ aircraft transects. Instead, spatial patterns of temporally averaged (seasonal/multi-annual)  $\text{NO}_2$  tropospheric columns have been analyzed under special conditions, resulting in lifetimes of 4 hours (12) up to a day (7, 17). The latter estimates are biased toward high values because they ignore effects of the satellite’s coarse spatial resolution.
- P. Levelt *et al.*, *IEEE Trans. Geosci. Rem. Sens.* **44**, 1093 (2006).
- K. F. Boersma *et al.*, *Atmos. Chem. Phys.* **7**, 2103 (2007).
- ECMWF, available at <http://www.ecmwf.int/research/ifsdocs/CY33r1/index.html>.
- Detailed methods are available as supporting material on Science Online.
- EDGAR, available at <http://edgar.jrc.ec.europa.eu/index.php>.
- Though specific emission inventories exist for various megacities (with highly variable quality), we present a comparison to the global EDGAR inventory, which is widely used in global atmospheric chemistry models.
- Available at <http://www.pnm.com/systems/4c.htm>.

**Acknowledgments:** The research leading to these results received funding from the European Union’s Seventh Framework Programme FP/2007-2011 within the project MEGAPOLI (grant 212520). We acknowledge the free use of tropospheric  $\text{NO}_2$  column data from the OMI sensor from [www.temis.nl](http://www.temis.nl). We thank the ECMWF for providing wind fields. EDGAR  $\text{NO}_x$  emissions for 2005 were provided by the European Commission, Joint Research Centre (JRC)—Netherlands Environmental Assessment Agency (PBL) (EDGAR version 4.1, <http://edgar.jrc.ec.europa.eu>, 2010). We thank S. Dörner for valuable assistance in processing ECMWF data.

#### Supporting Online Material

[www.sciencemag.org/cgi/content/full/333/6050/1737/DC1](http://www.sciencemag.org/cgi/content/full/333/6050/1737/DC1)  
Methods  
SOM Text  
Table S1  
Figs. S1 to S4

2 May 2011; accepted 3 August 2011  
10.1126/science.1207824

## Inbreeding Promotes Female Promiscuity

Łukasz Michalczyk,<sup>1</sup> Anna L. Millard,<sup>1</sup> Oliver Y. Martin,<sup>1,2</sup> Alyson J. Lumley,<sup>1</sup> Brent C. Emerson,<sup>1,3</sup> Tracey Chapman,<sup>1</sup> Matthew J. Gage<sup>1\*</sup>

The widespread phenomenon of polyandry (mating by females with multiple males) is an evolutionary puzzle, because females can sustain costs from promiscuity, whereas full fertility can be provided by a single male. Using the red flour beetle, *Tribolium castaneum*, we identify major fitness benefits of polyandry to females under inbreeding, when the risks of fertilization by incompatible male haplotypes are especially high. Fifteen generations after inbred populations had passed through genetic bottlenecks, we recorded increased levels of female promiscuity compared with noninbred controls, most likely due to selection from prospective fitness gains through polyandry. These data illustrate how this common mating pattern can evolve if population genetic bottlenecks increase the risks of fitness depression due to fertilization by sperm carrying genetically incompatible haplotypes.

It is unknown why females in the majority of species mate with multiple males (1, 2) particularly when complete fertility can be provided by a single male, no direct benefits come

from males apart from fertilizing sperm, and promiscuity can incur substantial costs for females (3). However, if postmating selection enables females to gain genetic benefits for their

offspring by promoting fertilization success of those sperm carrying more compatible paternal haplotypes (4, 5), polyandry may be favored. Studies of hybridizing species reveal the rapid evolution of molecular mechanisms that avoid fertilization by genetically less compatible sperm haplotypes (6). Furthermore, measures of reproductive dynamics within a species show that equivalent mechanisms exist at the gamete level to favor fertilization compatibility (7–12). These mechanisms may explain the evolution of polyandry, even in the face of costs to females that

<sup>1</sup>School of Biological Sciences, University of East Anglia, Norwich Research Park, Norwich NR4 7TJ, UK. <sup>2</sup>ETH Zurich, Institute of Integrative Biology, Universitätsstrasse 16, CHN J 11, 8092 Zurich, Switzerland. <sup>3</sup>Island Ecology and Evolution Research Group (IPNA-CSIC), C/Astrofísico Francisco Sánchez 3, 38206 La Laguna, Tenerife, Canary Islands, Spain.

\*To whom correspondence should be addressed. E-mail: [m.gage@uea.ac.uk](mailto:m.gage@uea.ac.uk)